Remote Doping of the Two-Dimensional-Electron-Gas State at the $LaInO_3/BaSnO_3$ Polar Interface

Juyeon Shin,[†] Young Mo Kim,[‡] Chulkwon Park,[†] and Kookrin Char[*]
Institute of Applied Physics, Department of Physics and Astronomy, Seoul National University, Seoul 08826, Korea

(Received 18 March 2020; revised manuscript received 31 March 2020; accepted 15 May 2020; published 26 June 2020)

We investigate the transport properties of a modified interface by intentionally inserting a nanometer-scale undoped $BaSnO_3$ spacer layer at the $LaInO_3/Ba_{1-x}La_xSnO_3$ interface, thereby creating remotely doped heterostructures. Both the carrier density (n_s) and the Hall mobility (μ_H) continuously decrease as the thickness of the $BaSnO_3$ spacer layer at the interface increases, indicating a changing electron-density profile as a function of the spacer thickness. We find the behavior is consistent with the recently proposed "interface-polarization" model by self-consistent one-dimensional Poisson-Schrödinger calculations. The decrease of n_s makes it difficult to see the effect of the spacer layer on the mobility in the remotely doped structures due to the simultaneous decrease of μ caused by the ineffective screening of the remote Coulomb scattering from ionized donors in addition to the threading dislocation scattering. Hence, we control the band bending continuously via the field effect with a fixed spacer-layer thickness, leading to observation of enhanced mobility (μ_{FE}) in the remotely doped 2DEG heterostructures in spite of high-density threading dislocations acting as the background charged impurities.

DOI: 10.1103/PhysRevApplied.13.064066

I. INTRODUCTION

Modulation doping in semiconductor heterostructures has played a key role in increasing the mobility of the charge carriers beyond the limit set by dopant scattering [1,2] and led to the discovery of the quantum Hall effect in a 2DEG [3] and the development of high-mobility transistors [4,5]. The conventional method of modulation doping is to remotely dope the larger-band-gap semiconductor in a band-gap-engineered heterostructure, causing significant band bending on both sides and resulting in a quantum-well structure at the surface of the smaller-band-gap semiconductor while keeping the dopant impurities away from the surface [6]. With the advent of new wide-band-gap semiconductors, such as GaN and ZnO, of intrinsic polar structures, the so-called polarization-doped 2DEG was realized [7,8] The polarization and band-gap discontinuity at the GaN/(Al,Ga)N interface [7,9] and the ZnO/(Mg,Zn)O interface [8,10] results in accumulation of mobile charges with 2DEG behavior at these interfaces. For more than a decade, 2DEG behavior at $SrTiO_3/LaAlO_3$ perovskite interfaces [11–13] has been studied extensively, and the polar structure of $LaAlO_3$ is believed to play an important role in formation of such a 2DEG [14,15], although efforts to investigate the exact mechanism behind it have been hampered by the instability of the $SrTiO_3$ surface [16–18].

Recently it was discovered that a transparent perovskite oxide semiconductor, $BaSnO_3$, has a wide band gap of 3.1 eV and high mobility of 320 $cm^2/V\ s$ at a three-dimensional carrier density (n_{3D}) of $8.0 \times 10^{19}\ cm^{-3}$ at room temperature when doped with La [19,20]. This corresponds to the highest value among all the three-dimensional semiconductors in the degenerately doped regime [21]. Many subsequent studies focused on the material properties [22,23] themselves and the demonstration of field-effect transistors (FETs) [24–27] based on a $BaSnO_3$ (BSO) channel, taking advantage of the excellent stability of its surface. However, the most unusual and interesting feature is the presence of the 2DEG-like state at the $LaInO_3$ (LIO)/$Ba_{1-x}La_xSnO_3$ (BLSO) polar interface [25,28,29]. The interface exhibits a sheet conductance enhancement up to several orders of magnitude, and the doping level of BSO was found to be a critical parameter; high two-dimensional carrier density (n_s) on the order of $10^{13}\ cm^{-2}$ requires slight La doping of the BSO layer to compensate for the deep acceptor states in BSO. We recently proposed an "interface-polarization" model to explain the experimental LIO thickness dependence of n_s [30]. Investigation of remotely doped 2DEG heterostructures will allow us to assess not only the validity of such a model but also the effectiveness of the remote-doping technique in oxide interfaces.

There has been extensive research on modulation doping based on compound III-V semiconductors, which

[*]kchar@phya.snu.ac.kr
[†]Present address: Samsung Electronics, Suwon, Korea.
[‡]Present address: SK Hynix Research, Icheon, Korea.

results in considerably reduced scattering in the ionized-impurity-scattering-dominated regime [1,2,4,5,31,32]. Consequently, the increase of μ leads to low *on*-state resistance and improved device performance in high-power and high-frequency applications. However, our remotely doped 2DEG heterostructure (LIO/BSO/BLSO) is different from the usual III-V modulation-doped heterostructures in which the undoped spacer layer and the doped layer are in the larger-band-gap material. The necessity for slight La doping in BSO comes from the fact that BSO has a high density of deep acceptors, N_{DA}, on the order of a 10^{19} cm^{-3}, mainly due to the threading dislocations and other cation vacancies. By moving the La doping away from the interface, one can find whether the proposed interface-polarization model is valid as well as whether the mobility can be increased in such a case. In the interface-polarization model, a large band bending is facilitated by the "interface polarization" in addition to the usual mismatch of the Fermi levels in conventional modulation-doped structures. Therefore, we add a nanometer-scale undoped spacer layer on the smaller-band-gap BSO side to keep the La dopants away from the accumulated free charges at the interface with LIO.

In this paper, we investigate the transport properties of remotely doped LIO/BSO (spacer layer)/BLSO heterostructures by taking advantage of the ability to control the exact doping in the BLSO system. The Hall measurement results reveal a continuous decrease of n_s and Hall mobility (μ_H) with increasing spacer-layer thickness, d. The manner in which n_s decreases is consistent with the simulation results obtained with the one-dimensional Poisson-Schrödinger equation using the interface-polarization model [30]. The simultaneous decrease of n_s and μ_H at the LIO/BSO polar interface as d increases is very likely due to the dislocation-limited transport in our current materials [22] as well as ineffective screening for remote charges by two-dimensional free carriers. To observe the electron-transport properties with continuous increasing of n_s at fixed d, FETs with a LIO gate oxide are fabricated. The continuous band bending caused by the field effect changes n_s and μ_{FE}, and leads to the observation of enhanced μ in our modulated structures.

All the samples are prepared by pulsed-laser deposition at 750 °C and an oxygen pressure of 0.1 Torr. The patterned layers are made with use of Si and stainless-steel stencil masks. The electrical measurements are performed with a Keithley 4200 SCS instrument along with a movable magnet with a magnitude of 0.5 T at room temperature. The n_s and $n_{3\mathrm{D}}$ profiles are calculated self-consistently with the use of a one-dimensional Poisson-Schrödinger program developed by Gregory Snider [30,33]. Extensive material characterization for the LIO/BSO interface is provided in our earlier publications, including reciprocal-space mapping [25,28,34], cross-section transmission electron microscopy, [28–30,34] and synchrotron scattering [35].

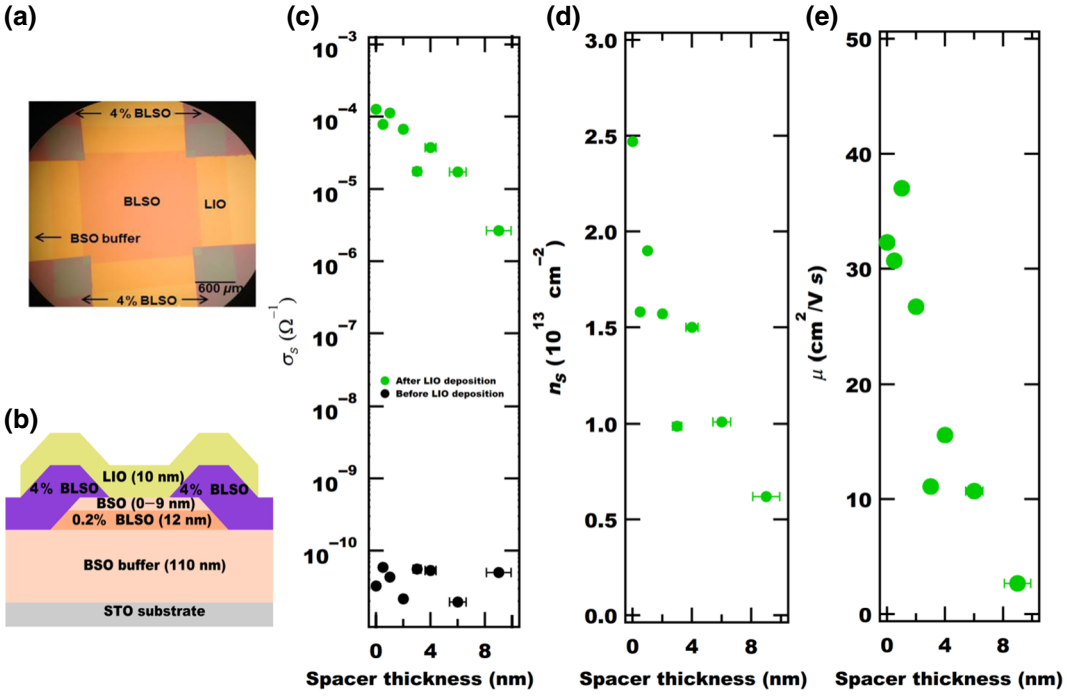

FIG. 1. Hall measurement results for the LIO/BSO (spacer)/0.2% BLSO interface with variation of the thickness of the spacer layer. (a) Top view of the structure pictured by an optical microscope. (b) Cross-section diagram of the structure (c)–(e) The sheet conductance, sheet carrier density, and mobility of the interface as a function of the spacer thickness.

Figures 1(a) and 1(b) show the lateral and vertical structures of the LIO/BSO/BLSO interface for the Hall measurement using the square Van der Pauw geometry. Further details on fabrication are available in our previous report on the LIO/BLSO polar interface [28]. The highly conductive 4% La–doped BSO is used as the electrodes. The distinguishing feature is an inserted undoped BSO spacer layer on top of the fixed donor density of the BLSO layer, so we can investigate the dependence of the transport properties on the distance to remote ionized-dopant impurities.

The sheet conductances (σ_s) as a function of d is shown in Fig 1(c). In each sample, we measure the sheet conductance σ_s before and after the LIO deposition, and find conductance enhancement of up to 6 orders of magnitude. Before LIO deposition, the samples are insulating with or without a spacer layer because the threading dislocations, with a large density of approximately 10^{11} cm^{-2}, trap substantial numbers of electrons, $N_{\mathrm{DA}} \approx 4 \times 10^{19}$–$6 \times 10^{19}$ cm^{-3} in BLSO films [22,30,34], acting as deep acceptors. However, the interface polarization doping after LIO deposition generates substantial band bending, resulting in a conducting interface. In our earlier report [28] we showed that the 2DEG at the LIO/BLSO interface does not originate from La diffusion or the creation of oxygen vacancies. As d increases, σ_s of the 2DEG continuously decreases, resulting in more than an-order-of-magnitude decrease at a spacer-layer thickness of 9 nm.

n_s and μ_H continuously decreases with increasing d as plotted in Figs. 1(d) and 1(e). n_s changes from 2.47×10^{13} to 6.20×10^{12} cm^{-2} and μ_H changes from 32.3 cm^2/V s to 2.68 cm^2/V s as d increases from 0 to 9 nm, which, at first sight, does not seem to be the desired effect of the spacer layer and remote doping. The carriers originating from the smaller-band-gap BLSO layer are drawn to the interface by the polarization, and thereby the undoped spacer layer decreases n_s. This is different from the conventional modulation-doped structures of III-V semiconductors [36], in which diffusion of the electrons from the larger-band-gap material is hardly hindered by insertion of a spacer layer. The first possible origin for the decrease of μ_H with d is that the Coulomb scattering by the La dopant is not dominant in transport, reducing the advantages of a remotely doped structure. Transport in BLSO film is limited by threading dislocations [19–22], and a recent FET experiment [27] on BSO found a dependence of $\mu \propto n_s^{\gamma}$, where $\gamma \cong 1.5$, similarly to a 2DEG in GaN [37]. Another possibility is that the screening for remote charges by two-dimensional free carriers is not very effective; higher n_s results in higher kinetic energy and μ. Coulomb scattering by doped ionized impurities for two-dimensional carriers has a dependence of $\mu \propto n_s^{\gamma}$, where $\gamma = 1 - 1.7$, as reported in a 2DEG of Si and compound semiconductors [38–40]. Therefore, μ enhancement in a remotely doped structure is negated by the decrease of n_s caused by the inserted spacer layer. This is reinforced by the fact that μ_H remains similar despite an up to 36% decrease of n_s in the d range from 0 to 2 nm, although μ_H decreases sharply from $d = 3$ nm. This suggests that μ of the remotely doped structure may be enhanced if n_s is supported by other means (e.g., by the field effect).

We report the calculated band bending of the LIO/BSO/BLSO structure and the three-dimensional free-carrier density distribution in the growth direction in Figs. 2(a) and 2(b). The dimensions of the structure are given in Fig. 1(b). The values of the band gap and the band offset are based on the band alignment reported in our first paper on the LIO/BLSO polar interface [28]. We set $m^* = 0.42 m_0$ for the conduction band of BSO [41], while its s-like band structure is conducive to use of the one dimensional Poisson-Schrödinger equation. As the densities of the La donors (N_d in BLSO) and the deep acceptors (N_{DA} in both BLSO and BSO) we use 2.87×10^{19} and 4×10^{19} cm^{-3}, respectively, with Ohmic boundary conditions [30]. Because the threading dislocations trap electrons in BLSO films [22], deep acceptor levels near the center of the band gap are imposed and the value is based on our previous Hall results as a function of La doping of MgO substrates [34]. We set the interface polarization P in LIO to be 65, 65, 25, and 10 μC/cm^2 in each of the four unit cells in the interfacial LIO layer along with a deep donor density (N_{DD}) in LIO of about 2×10^{20} cm^{-3} to satisfy the experimental n_s value as a function of LIO thickness, as described in detail in Ref. [30]. Such interface polarization and deep donor density in LIO enables the generation of a confined well at the interface, as shown in Fig. 2(a). The width and depth of the well decrease with increasing spacer thickness, which is well illustrated in the inset in Fig. 2(a) and in Fig. S1 [42]. The free-carrier density at the interface continuously decreases, as shown in Fig. 2(b), for a thickness range of 1–2 nm. The peak $n_{3\mathrm{D}}$ decreases from 2.03×10^{20} to 7.88×10^{19} cm^{-3} as the spacer-layer thickness increases from 0 to 9 nm. Recent thermoelectric power measurements [43] of three-dimensional and two-dimensional BSO suggested the confinement length to be about 1 nm, which is consistent with our simulation and a general value of the dielectric constant of about 20 in BSO. Our simulation also tells us that only one subband is occupied in our LIO/BSO case; $E_2 - E_1 = 0.3$ eV and $E_F - E_1 = 0.1$ eV. The large density of states, $m^*/\pi\hbar^2$, of about 2×10^{14} cm^{-2} eV^{-1} in BSO can accommodate a carrier density on the order of 10^{13} cm^{-2} in a 2DEG with single-subband occupation. The plot in Fig. 2(c) compares n_s from the experimental results in Fig. 1 with n_s from the calculation with varying spacer thickness d for three different deep acceptor densities (N_{DA}) in BSO. The overall dependence of n_s on d agrees best in the case of $N_{\mathrm{DA}} = 5 \times 10^{19}$ cm^{-3}. This N_{DA} value on $SrTiO_3$ substrates is consistent with our recent

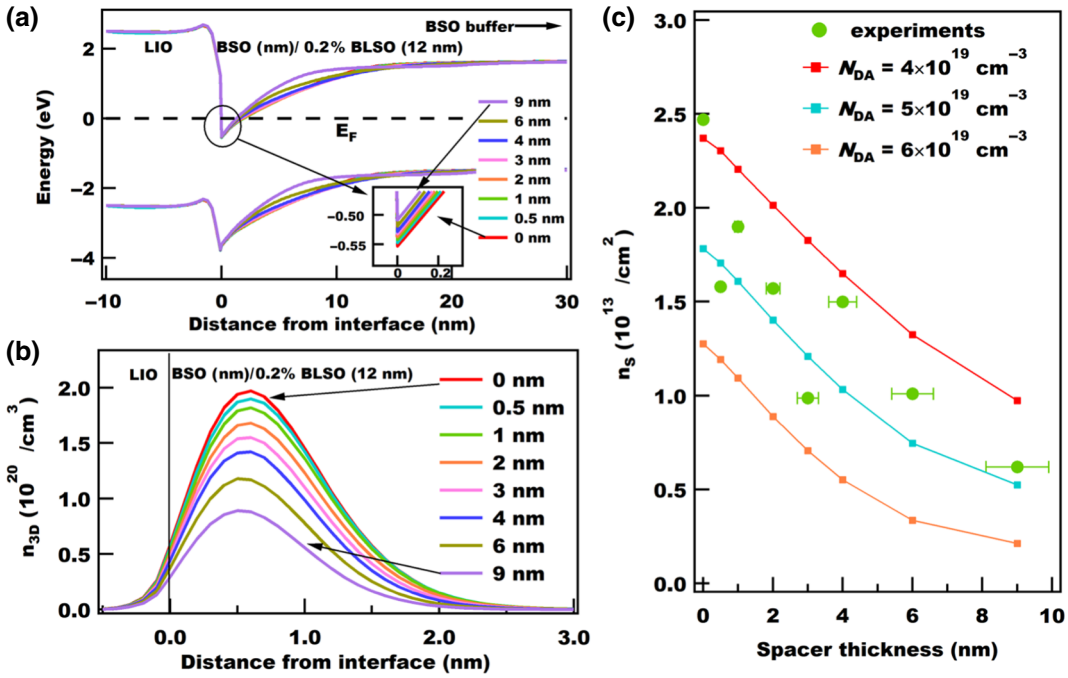

FIG. 2. Self-consistent Poisson-Schrödinger calculation for the LIO/BSO (spacer)/0.2% BLSO interface with varying the thickness of the spacer layer. (a) Conduction-band and valence-band edge profiles (the dotted line is a Fermi level) and (b) the electron concentration n_{3D} as a function of distance from the interface assuming $N_{DA}=4\times10^{19}$ cm^{-3} in BSO and BLSO. (c) Experimental and simulated results for n_s as a function of the spacer thickness with three slight variations of N_{DA}.

report [30]. Furthermore, most of fluctuation of n_s as a function of d are likely to come from the variation of the deep acceptor density in each sample due to the slightly different surface quality of the substrate and the slight change in the pulsed-laser-deposition process.

Because n_s strongly depends on d as in Fig. 1, we fabricate the field-effect device to control n_s continuously at fixed d. This also reduces the error coming from the fluctuation of the density of the deep acceptor states in each sample. Top and vertical views of the structures are shown in Figs. 3(a) and 3(b). Details of the fabrication method are given in our previous paper on FETs based on a BSO channel [25]. Our previous study of FETs using epitaxial BSO and LIO demonstrates the excellent interface property [25]. We use highly conductive 4% La-doped BSO for the electrodes and 244-nm-thick LIO as the gate oxide. We fabricate four transistors with LIO/0.2% BLSO, LIO/BSO(9 nm)/0.2% BLSO, LIO/0.4% BLSO, and LIO/BSO(9 nm)/0.4% BLSO interfaces. The channel length (L) and the channel width (W) are around 140 and 110 μm, respectively. Although the conductance of the Hall structure (10-nm-thick LIO) with a spacer layer is lower by more than an order of magnitude than that without a spacer layer when measured by four point contacts, structures with and without a spacer layer in FET devices (244-nm-thick LIO) have similar σ_s, about 1 MΩ, since FETs are made with only two point contacts and the contact resistances are much higher than the device resistance measured by the four-point method due to the very small cross-section contact area.

The typical output and transfer characteristics for a transistor with and without a spacer layer with the same 0.2% BLSO channel layer are plotted in Figs. 3(c) and 3(d). The properties of the 0.4% BLSO channel layer are shown in Fig. S2. The drain-source current (I_{DS}) versus the drain-source voltage (V_{DS}) at various gate-source voltages (V_{GS}) s indicates that the devices operate in an n-type accumulation mode and that pinch-off occurs at high V_{DS}. The transfer characteristics in Fig. 3(d) represent I_{DS} versus V_{GS} in the linear region ($V_{DS}=1$ V), as confirmed in Fig. 3(c). From this result, μ_{FE} is evaluated by use of the relation $\mu_{FE}=g_m[L/(C_{ox}WV_{DS})]$, where $g_m=\partial I_{DS}/\partial V_{GS}$ and $C_{ox}$is the capacitance per unit area, and the subthreshold swing (S) is evaluated by the relation $S=(\partial \log I_{DS}/\partial V_{GS})^{-1}$. In all devices, we apply a gate-source voltage while keeping the gate-source current (I_{GS}) 1–2 orders of magnitude lower than I_{DS} to avoid breakdown of the gate oxide. I_{DS} reaches around 10^{-4} A in both cases in the highly accumulated region. In devices with a spacer layer, μ_{FE} is higher than in devices without a spacer layer for V_{GS} above approximately 13 V. This phenomenon occurs also for FETs with a 0.4% BLSO channel layer (Fig. S2). μ_{FE} with a 9-nm spacer shows a steeper increase for V_{GS} above 17 V.

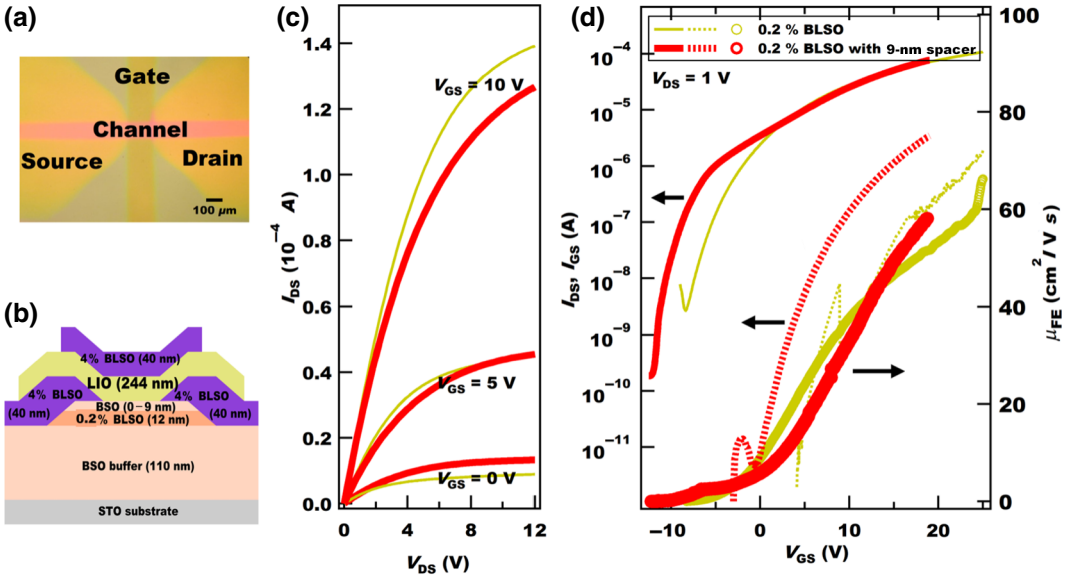

FIG. 3. Typical field-effect results for LIO/0.2% La–doped BSO and LIO/BSO(9 nm)/0.2% BLSO interfaces. (a) Top view of the device pictured by an optical microscope. (b) Cross-section diagram of the device. (c) Output characteristics of the devices and (d) transfer characteristics of the devices in the linear region (V_{DS}= 1 V) with 0.2% BLSO.

The threshold voltage (V_{th}) is −1.45 V without a spacer and 0.2 V with a spacer for a 0.2% BLSO channel and is −1.2 V without a spacer and 4 V with a spacer for a 0.4% BLSO channel as shown in Fig. S3 by extrapolation of the linearly fitted line of $I_{DS}^{1/2}$ versus V_{GS} according to the standard square-law theory of FETs; namely, $I_{DS,sat} \propto (V_{GS} - V_{th})^2$, where $I_{DS,sat}$ is the saturation current [25,44]. It is interesting that the spacer FET in Fig. S3(d) shows am additional linear decrease in the subthreshold region. In such a subthreshold region, which is related to the diffusion current in a MOSFET and to the pinch-off of both the drift current and the hopping mechanism in a thin-film transistor through the trap states, the relations $I_{DS} \propto \exp(qV_{GS}/nk_BT)$ and $S = n(k_BT/q)\ln 10$ hold, where k_B, T, q, and n are the Boltzmann constant, the absolute temperature, the electron charge, and a factor specific to a model, respectively [44,45]. In our remotely doped structures, there is a possibility that the La-doped layer below the spacer layer contributes small parallel conduction in the region of negative or small positive bias of V_{GS}, where n_s at the LIO/BSO interface is small. This is manifested in the unusual transport in Figs. 3(c) and S2(a), where I_{DS} of the FET with a spacer is larger than that of the FET without a spacer at small V_{GS}, but I_{DS} of the FET without a spacer eventually becomes larger than that of the FET with spacer at high V_{GS}, leading to higher *off* -state currents in the case of FETs with a spacer. Similar behavior is seen in the transfer curves in Figs. 3(d) and S2(b), and it is more pronounced for the more-highly-doped 0.4% BLSO channel layer. The analysis of the subthreshold region in our remotely doped structure with two parallel conduction channels, which usually arises in the highly accumulated region by excessive forward bias in a conventional MOSFET [46], needs more-careful study, and the details are beyond the scope of the subject in this paper. On the other hand, S values for FETs with spacers are smaller (approximately 1/3) than those of their no-spacer counterparts in both the 0.2% BLSO channel and the 0.4% BLSO channel, showing the advantage of the absence of La dopants near the interface.

Figure 4 shows μ_{FE} versus n_s in our four types of FETs, where n_s is evaluated from the relation $n_s = C_{ox}/q(V_{GS} - V_{th})$. If dislocation scattering is dominant, which depends on n_s and not on the doping rate of La ionized impurity, all four curves should have the same slope and be on the same line, assuming they all have the same density of dislocations [27,47]. FETs with a 0.4% BLSO layer have smaller μ_{FE} than those with a 0.2% BLSO layer, an indication that La dopants exert a measurable effect in our case. However, μ_{FE} of the FET with a spacer layer is higher than that without a spacer layer for each La doping rate. The continuous control of n_s enables us to determine the enhancement of μ in the remotely doped structures, albeit a small effect. This confirms the difficulty of interpreting the mobility results deduced from Hall measurements in Fig. 1, in which the decrease of μ due to the decrease of n_s screens the small enhancement of μ_{FE} when a spacer layer is inserted. Moreover, the distinctive feature between the FET with a spacer and the FET without a spacer is their slope; γ in the relation $\mu \propto n_s^{\gamma}$ changes from 0.65 to 0.75 for the 0.2% BLSO FET after insertion of a spacer layer and changes from 1.06 to 1.26 for the 0.4% BLSO FET. Larger γ

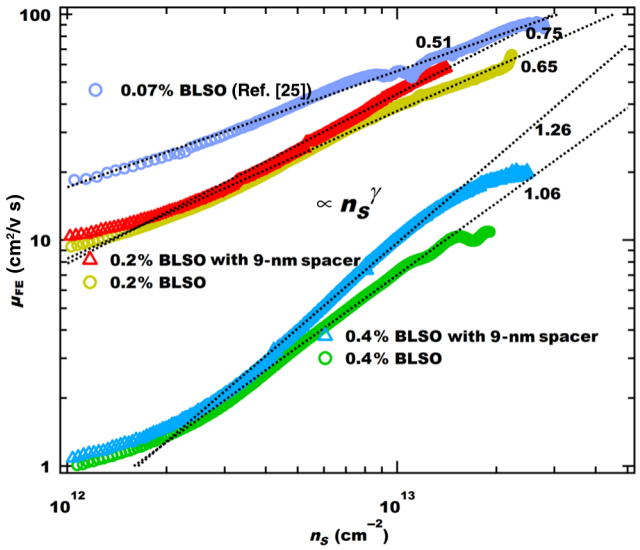

FIG. 4. Field-effect mobility as a function of the sheet carrier density in the field-effect devices. The dashed lines represent $\mu \propto n_s^{\gamma}$ fitted lines. The numbers represent γ values for each line.

values with increasing d are found in the GaAs/(Al,Ga)As modulation-doped structure, especially $\mu \propto n_s^{1.5}/N_{i,\,\mathrm{sheet}}$ where $N_{i,\mathrm{sheet}}$ is the δ-doped ionized sheet carrier density in the unscreened limit of very large d [39,40,48]. On the other hand, the enhancement of μ_{FE} is small in spite of the 9-nm spacer-layer thickness, which is much larger than $1/k_F$ [$k_F = (2\pi n_s)^{1/2}$, Fermi wave number in two dimensions] of 1–2 nm for $n_s \cong 10^{13}\,\mathrm{cm}^{-2}$. This makes μ_{FE} depend more on the La doping rate, yielding smaller μ_{FE} for all the FETs with a spacer than for the 0.07% BLSO FET. Also the decrease of slope with reducing La doping indicates that there is a mechanism that sets an upper bound of transport in the LIO/BLSO polar interface by other origins for scattering, such as background charged impurities.

The enhancement of μ by remote doping is significant in the case when the remote ionized-impurity scattering is dominant in transport; the dramatic increase of μ is well reported in GaAs/(Al, Ga)As structures of high crystallinity [2]. However, it is known that unintentional background charged impurities lower μ in the 2DEG of GaAs/(Al, Ga)As and Si/Si-Ge [49,50]. For the GaN/(Al, Ga)N interface, which has a large transport dependence on the substrate [51], μ does not depend on the donor density of the charge-supplying layer [52], indicating the dominant scattering is not due to the remote ionized-dopant scattering. BSO has a large density of trap states mainly originating from dislocations, which suggests that further studies on reducing such dislocation density will result in much-greater mobility in the remotely doped LIO/BSO/BLSO interface.

In summary, we study the transport properties of the LIO/BSO (spacer)/BLSO interface. The n_s versus d (the spacer-layer thickness) relation is found to be consistent with the interface-polarization model by Poisson-Schrödinger simulation. The Hall measurement of heterostructures with varying d was not sufficient to see the enhanced mobility when a spacer layer is inserted, since n_s sharply decreases with d. However, by use of FETs, which enables us to continually control n_s at fixed d, the enhancement of μ_{FE} in remotely doped structures is observed. Our results will contribute to understanding and further advance of the LIO/BLSO polar interface for fundamental science at low temperatures as well as high-power and high-frequency electronics applications of such an interface.

ACKNOWLEDGMENTS

This work was supported in part by the Samsung Science and Technology Foundation under Project No. SSTF-BA1402-09. This material is also based on work supported by the Air Force Office of Scientific Research under Grant No. FA9550-16-1-0192. Part of this study was performed with use of facilities at the IBS Center for Correlated Electron Systems, Seoul National University.

[1] R. Dingle, H. L. Stormer, A. C. Gossard, and W. Wiegmann, Electron mobilities in modulation-doped semiconductor heterojunction superlattices, Appl. Phys. Lett. **33**, 665 (1978).
[2] D. G. Schlom and L. N. Pfeiffer, Oxide electronics: Upward mobility rocks!, Nature Mater. **9**, 881 (2010).
[3] D. C. Tsui, H. L. Stormer, and A. C. Gossard, Two-dimensional Magnetotransport in the Extreme Quantum Limit, Phys. Rev. Lett. **48**, 1559 (1982).
[4] T. Mimura, S. Hiyamizu, T. Fujii, and K. Nanbu, A new field-effect transistor with selective doped GaAs/n-Al_x Ga_{1-x}As heterojunctions, Jpn. J. Appl. Phys. **19**, L225 (1980).
[5] R. Dingle, New high-speed III–V devices for integrated circuits, IEEE Trans. Electron. Dev. **ED-31**, 1662 (1984).
[6] J. H. Davis, *The Physics of low Dimensional Semiconductors* (Cambridge University Press, New York, 1998).
[7] O. Ambacher, J. Smart, J. R. Shealy, N. G. Weimann, K. Chu, M. Murphy, W. J. Schaff, L. F. Eastman, R. Dimitrov, L. Wittmer, M. Stutzmann, W. Rieger, and J. Hilsenbeck, Two-dimensional electron gases induced by spontaneous and piezoelectric polarization charges in N- and Ga-face AlGaN/GaN heterostructures, J. Appl. Phys. **85**, 3222 (1999).
[8] H. Tampo, H. Shibata, K. Matsubara, A. Yamada, P. Fons, S. Niki, M. Yamagata, and H. Kanie, Two-dimensional electron gas in Zn polar ZnMgO/ZnO heterostructures grown by radical source molecular beam epitaxy, Appl. Phys. Lett. **89**, 132113 (2006).

[9] M. J. Manfra, K. W. Baldwin, A. M. Sergent, K. W. West, R. J. Molnar, and J. Caissie, Electron mobility exceeding 160000 cm^2/Vs in AlGaN/GaN heterostructures grown by molecular-beam epitaxy, Appl. Phys. Lett. **85**, 5394 (2004).

[10] A. Tsukazaki, S. Akasaka, K. Nakahara, Y. Ohno, H. Ohno, D. Maryenko, A. Ohtomo, and M. Kawasaki, Observation of the fractional quantum hall effect in an oxide, Nature Mat. **9**, 889 (2010).

[11] A. Ohtomo and H. Y. Hwang, A high-mobility electron gas at the $LaAlO_3/SrTiO_3$ heterointerface, Nature **427**, 423 (2004).

[12] S. Thiel, G. Hammerl, A. Schmehl, C. W. Schneider, and J. Mannhart, Tunable quasi-two-dimensional electron gases in oxide heterostructures, Science **313**, 1942 (2006).

[13] N. Reyren, S. Thiel, A. D. Caviglia, L. Fitting Kourkoutis, G. Hammerl, C. Richter, C. W. Schneider, T. Kopp, A.-S. Rüetschi, D. Jaccard, M. Gabay, D. A. Muller, J.-M. Triscone, and J. Mannhart, Superconducting interfaces between insulating oxides, Science **317**, 1196 (2007).

[14] Z. Q. Liu, C. J. Li, W. M. Lu, X. H. Huang, Z. Huang, S.W. Zeng, X. P. Qiu, L. S. Huang, A. Annadi, J. S. Chen, J. M. D. Coey, T. Venkatesan, and Ariando, Origins of the two-dimensional electron gas at $LaAlO_3/SrTiO_3$ interfaces: The role of oxygen vacancies and electron reconstruction, Phys. Rev. X **3**, 021010 (2013).

[15] L. Yu and A. Zunger, A polarity-induced defect mechanism for conductivity and magnetism at polar-nonpolar oxide interfaces, Nat. Commun. **5**, 5118 (2014).

[16] G. Herranz, M. Basletic, M. Bibes, C. Carretero, E. Tafra, E. Jacquet, K. Bouzehouane, C. Deranlot, J.-M. Hamzic, A. Barthélémy Broto, and A. Fert, High Mobility in $LaAlO_3/SrTiO_3$ Heterostructures: Origins, Dimensionality, and Perspertives, Phys. Rev. Lett. **98**, 216803 (2007).

[17] A. Kalabukhov, Y. A. Boikov, I. T. Serenkov, V. I. Sakharov, J. Borjesson, N. Ljustina, E. Olsson, D. Winkler, and T. Claeson, Improved cationic stoichiometry and insulating behavior at the interface of $LaAlO_3/SrTiO_3$ formed at high oxygen pressure during pulsed-laser deposition, EPL (Europhysics Lett.) **93**, 37001 (2011).

[18] A. Ohtomo and H. Y. Hwang, Growth mode control of the free carrier density in $SrTiO_{3-\delta}$ films, J. Appl. Phys. **102**, 083704 (2007).

[19] H. J. Kim, U. Kim, H. M. Kim, T. H. Kim, H. S. Mun, B.-G. Jeon, K. T. Hong, W.-J. Lee, C. Ju, K. H. Kim, and K. Char, High mobility in a stable transparent perovskite oxide, Appl. Phys. Express **5**, 061102 (2012).

[20] H. J. Kim, U. Kim, T. H. Kim, J. Kim, H. M. Kim, B.-G. Jeon, W.-J. Lee, H. S. Mun, K. T. Hong, J. Yu, K. Char, and K. H. Kim, Physical properties of transparent perovskite oxides $(Ba, La)SnO_3$ with high electrical mobility at room temperature, Phys. Rev. B **86**, 165205 (2012).

[21] U. Kim, Ph. D. Thesis, Seoul National Univ., 2015.

[22] H. Mun, U. Kim, H. M. Kim, C. Park, T. H. Kim, H. J. Kim, K. H. Kim, and K. Char, Large effects of dislocations on high mobility of epitaxial perovskite $Ba_{0.96}La_{0.04}SnO_3$ films, Appl. Phys. Lett. **102**, 252105 (2013).

[23] S. Raghavan, T. Schumann, H. Kim, J. Y. Zhang, T. A. Cain, and S. Stemmer, High-mobility $BaSnO_3$ grown by oxide molecular beam epitaxy, APL Mater. **4**, 016106 (2016).

[24] C. Park, U. Kim, C. J. Ju, J. S. Park, Y. M. Kim, and K. Char, High mobility field effect transistor based on $BaSnO_3$ with Al_2O_3 gate oxide, Appl. Phys. Lett. **105**, 203503 (2014).

[25] U. Kim, C. Park, T. Ha, Y. M. Kim, N. Kim, C. Ju, J. Park, J. Yu, J. H. Kim, and K. Char, All-perovskite transparent high mobility field effect using epitaxial $BaSnO_3$ and $LaInO_3$, APL Mater. **3**, 036101 (2015).

[26] Y. M. Kim, C. Park, T. Ha, U. Kim, N. Kim, J. Shin, Y. Kim, J. Yu, J. H. Kim, and K. Char, High-k perovskite gate oxide $BaHfO_3$, APL Mater. **5**, 016104 (2017).

[27] K. Fujiwara, K. Nishihara, J. Shiogai, and A. Tsukazaki, Enhanced electron mobility at the two-dimensional metallic surface of $BaSnO_3$ electric-double-layer transistor at low temperatures, Appl. Phys. Lett. **110**, 203503 (2017).

[28] U. Kim, C. Park, Y. M. Kim, J. Shin, and K. Char, Conducting interface states at $LaInO_3/BaSnO_3$ polar interface controlled by Fermi level, APL Mater. **4**, 071102 (2016).

[29] Y. Kim, Y. M. Kim, J. Shin, and K. Char, $LaInO_3/BaSnO_3$ polar interface on MgO substrates, APL Mater. **6**, 096104 (2018).

[30] Y. M. Kim, T. Markurt, Y. Kim, M. Zupancic, J. Shin, M. Albrecht, and K. Char, Interface polarization model for a 2-dimensional electron gas at the $BaSnO_3/LaInO_3$ interface, Sci. Rep. **9**, 16202 (2019).

[31] J. J. Harris, C. T. Foxon, D. E. Lacklison, and K. W. J. Barnham, Scattering mechanisms in (Al, Ga)As/GaAs 2DEG structures, Superlattices Microstruct. **2**, 563 (1986).

[32] S. J. Pearton, *GaN and Related Materials II* (Gordon and Breach Science Publishers, Singapore, 2000).

[33] G. Snider, 1D Poisson-Schrödinger solver program, https://www3.nd.edu/∼gsnider/.

[34] J. Shin, Y. M. Kim, Y. Kim, C. Park, and K. Char, High mobility $BaSnO_3$ films and field effect transistors on non-perovskite MgO substrate, Appl. Phys. Lett. **109**, 262102 (2016).

[35] C. Lau, Y. Kim, S. Albright, K. Char, C. H. Ahn, and F. J. Walker, Structural characterization of the $LaInO_3/BaSnO_3$ interface via synchrotron scattering, APL Mater. **7**, 031108 (2019).

[36] J. V. DiLorenzo, R. Dingle, M. Feuer, A. C. Gossard, R. Hendel, J. C. M. Hwang, A. Kastalsky, V. G. Keramidas, R. A. Kiehl, and P. O'Connor, Material and device considerations for selectively doped heterojunction transistors, IEDM Tech. Dig. **25**, 578 (1982).

[37] D. Delageveaudeuf and N. T. Linh, Metal-(n) AlGaAs-GaAs two-dimensional electron gas FET, IEEE Trans. Electron. Dev. **ED-29**, 955 (1982).

[38] T. Ando, A. B. Fowler, and F. Stern, Electronic properties of two-dimensional systems, Rev. Mod. Phys. **54**, 437 (1982).

[39] T. Ando, Self-consistent results for a $GaAs/Al_xGa_{1-x}As$ heterojunction. II. Low temperature mobility, J. Phys. Soc. Jpn. **51**, 3900 (1982).

[40] K. Hirakawa and H. Sakaki, Mobility of the two-dimensional electron gas at selectively doped n-type $Al_xGa_{1-x}As/GaAs$ heterojunctions with controlled electron concentrations, Phys. Rev. B **33**, 8291 (1986).

[41] U. Kim, C. Park, T. Ha, R. Kim, H. S. Mun, H. M. Kim, H. J. Kim, T. H. Kim, N. Kim, J. Yu, K. H. Kim, J. H. Kim, and K. Char, Dopant-site-dependent scattering by

dislocations in epitaxial films of perovskite semiconductor $BaSnO_3$, APL Mater. **2**, 056107 (2014).

[42] See Supplemental Material at http://link.aps.org/supplemental/10.1103/PhysRevApplied.13.064066 for more detailed electrical data.

[43] A. V. Sanchela, T. Onozato, B. Feng, Y. Ikuhara, and H. Ohta, Thermopower modulation clarification of the intrinsic effective mass in transparent oxide semiconductor $BaSnO_3$, Phys. Rev. Materials **1**, 034603 (2017).

[44] Y. Tsividis and C. McAndrew, *Operation and Modeling of the MOS Transistor* (Oxford University Press., New York, 2011).

[45] H. Marien, M. Steyaert, and P. Heremans, *Analog Organic Electronics* (Springer Science, New York, 2013).

[46] E. F. Schubert, K. Ploog, H. Dambkes, and K. Heime, Selectively doped n-$Al_xGa_{1-x}As$/GaAs heterostructures with high-mobility two-dimensional electron gas for field effect transistors, Appl. Phys. A **33**, 63 (1984).

[47] M. J. Manfra, L. N. Pfeiffer, K. W. West, H. L. Stormer, K. W. Baldwin, J. W. P. Hsu, D. V. Lang, and R. J. Molnar, High-mobility AlGaN/GaN heterostructures grown by molecular-beam epitaxy on GaN templates prepared by hybride vapor phase epitaxy, Appl. Phys. Lett. **77**, 2888 (2000).

[48] S. D. Sarma, E. H. Hwang, S. Kodiyalam, L. N. Pfeiffer, and K. W. West, Transport in two-dimensional modulation-doped semiconductor structures, Phys. Rev. B **91**, 205304 (2015).

[49] E. H. Hwang and S. D. Sarma, Limit to two-dimensional mobility in modulation-doped GaAs quantum structures: How to achieve a mobility of 100 million, Phys. Rev. B **77**, 235437 (2008).

[50] X. Mi, T. M. Hazard, C. Payette, K. Wang, D. M. Zajac, J. V. Cady, and J. R. Petta, Magnetotransport studies of mobility limiting mechanisms in undoped Si/SiGe heterostructures, Phys. Rev. B **92**, 035304 (2015).

[51] R. Gaska, M. S. Shur, A. D. Bykhovski, A. O. Orlov, and G. L. Snider, Electron mobility in modulation-doped AlGaN-GaN heterostructures, Appl. Phys. Lett. **74**, 287 (1999).

[52] M. Marso, J. Bernat, P. Javorka, and P. Kordos, Influence of a carrier supply layer on carrier density and drift mobility of AlGaN/GaN/SiC high-electron-mobility transistors, Appl. Phys. Lett. **84**, 2928 (2004).